Int. J. Electrochem. Sci., 15 **(2020)** 10653 – 10663, doi: 10.20964/2020.11.33

International Journal of
ELECTROCHEMICAL
SCIENCE
www.electrochemsci.org

Short Communication

Effect of Surfactants on the Electrochemical Performance of FeS_2 Synthesized by Hydrothermal Method

Huili Jia[1], *Jianping Li*[2,*], *Li Wang*[2,4], *Zhaoming Huang*[3], *Jing Xu*[3,**]

[1] School of Automotive Engineering, Wuhu Institute of Technology, Wuhu, 241006, China;
[2] Automotive & Transportation Engineering, Shenzhen Polytechnic, Shenzhen, 518055, China;
[3] School of Mechanical Engineering, Wanjiang University of Technology, Ma'anshan, 243031, China;
[4] School of Electromechanical and Automotive Engineering, Xuancheng Vocational and Technical College, Xuancheng, 242000, China.
[*]E-mail: szyljp0170@szpt.edu.cn (J. Li), shiliu1109@126.com (J. Xu)

Received: 3 August 2020 / *Accepted:* 24 August 2020 / *Published:* 30 September 2020

FeS_2 is a potential electrode material because of its abundant resources, low price and environmental protection. However, there are some problems when using FeS_2 as an electrode material, such as poor reversibility and side reactions. In this study, the effects of different surfactants on the morphology and electrochemical properties of FeS_2 synthesized by the hydrothermal method were discussed. Results show that FeS_2 synthesized without surfactant is composed of pyrite and marcasite; FeS_2 prepared by adding polyvinyl pyrrolidone (PVP) is cubic pyrite, and PVP inhibits the formation of marcasite and promotes the crystal growth of pyrite; Polyethylene glycol (PEG) is similar to PVP, but PEG promotes crystal growth excessively and forms micron-scale flower-like spherical particles. FeS_2 with hexadecyl trimethyl ammonium bromide (CTAB) is cubic pyrite with the morphology of micro toothed spherical particles. CV and EIS showed that the reactions of the FeS_2 electrode prepared by adding PVP, surfactant-free, CTAB and PEG were reversible, and the specific capacities were 82.20 F/g, 141.03 F/g, 191.68 F/g and 134.37 F/g at 5 mV/s, respectively. The electrochemical performance of FeS_2 electrode material with CTAB was excellent, which was attributed to its lower charge transfer impedance and fast ion diffusion.

Keywords: supercapacitor; FeS_2; surfactant; electrochemical property

1. INTRODUCTION

With the improvement of the economic level and the progress of science and technology, people's demand for high-performance, pollution-free batteries continues to grow [1-3]. More and more electric vehicles and hybrid electric vehicles, including a large number of portable electronic devices, have put

forward higher requirements on the performance of energy storage devices. Lithium-ion batteries with good safety performance and high energy density are used in portable electronic equipment [4-8].

A supercapacitor is a type of energy storage device with the characteristics of the chemical battery and traditional static capacitance [9-11]. Compared with batteries, supercapacitors have high power density; for traditional capacitors, supercapacitors have high energy density. Supercapacitors are divided into double-layer capacitors and Faraday capacitors according to different energy storage mechanisms [12, 13]. In short, the energy storage of electric double-layer capacitors does not occur chemical reactions but is achieved through electrochemical polarization of electrolyte solution, and the process is reversible; the energy storage mechanism of Faraday capacitors is similar to that of secondary batteries, which converts electrical energy into chemical energy achieved through oxidation and reduction reactions [14-16].

Transition metal sulfides have unique nanostructures and electrical properties, so they have a wider range of applications. However, metal sulfides have high surface energy and are prone to agglomeration, which affects their electrochemical performance [9]. Therefore, researchers try to use excessive metal sulfides and matrix materials to form composite materials and use synergistic effects to improve their performance [9, 10, 17]. For example, Pei et al. [17] used a two-step self-assembly method to synthesize a graphene aerosol-supported FeS_2 composite material (GA-FeS_2). The electrochemical performance test showed that the specific capacitance at 0.5 A/g was 313.6 F/g, which is almost twice that of FeS_2 (163.5 F/g). The composite material has excellent cycle performance (capacity retention rate of 88.2% after 2000 cycles at 10 A/g) and low charge transfer resistance. The symmetrical supercapacitor assembled using GA-FeS_2 has a wide potential range and an energy density of up to 22.86 Wh/kg. Javed et al. [18] studied flexible solid-state supercapacitors based on carbon paper FeS_2 nanospheres. The electrochemical performance test showed that the specific capacity is 484 F/g at 5 mV/s, which has excellent cycle stability. After 5000 cycles, the post-capacity retention rate is 95.7%. The energy density of the supercapacitor is 44 Wh/kg, power density is 175 W/kg, and the coulomb efficiency is 97%.

FeS_2 in the transition metal sulfides is rich in resources, low in price, environmentally friendly and has excellent electrochemical performance (theoretical capacity of 890 mA h g^{-1}), so it was widely used as eletrode materials for lithium batteries in the early stage [19, 20]. FeS_2 as electrode material has the following two problems: (i) the reversibility of the electrode reaction is poor. FeS_2 could not be formed by reverse reaction at room temperature; (ii) side reaction occurred between FeS_2 and electrolyte. The mixture of FeS_y and S is formed during the charging process. S is easily dissolved in the electrolyte, resulting in the loss of capacity and poor cycling. Therefore, the improvement of electrode performance should be to promote the electrode reaction kinetics process, improve the stability of the electrode in the reaction process, modify the contact interface between active substances and electrolyte, and reduce the formation of side reactions [21]. In this study, FeS_2 with different morphologies and structures were synthesized by modifying FeS_2 with different surfactants (polyvinyl pyrrolidone (PVP), polyethylene glycol (PEG), hexadecyl trimethyl ammonium bromide (CTAB)), and then the effect of FeS_2 on electrochemical performance was studied.

2. EXPERIMENTAL

2.1. Preparation of FeS_2.

FeS_2 samples were prepared by the hydrothermal method. First, 1668 mg ferrous sulfate heptahydrate and 1488 mg sodium thiosulfate pentahydrate were dissolved in 25 ml deionized water and mixed. 200 mg of sublimated sulfur was added to the above solution, and ultrasonic oscillation was performed at room temperature for 30 minutes. Then, the solution was added to a stainless steel reactor, kept in 200 ℃ electric blast drying oven for 24 h, and then cooled to room temperature. The prepared samples were washed with absolute ethanol, carbon disulfide, and deionized water for three times, and then dried in a vacuum drying oven at 80 ℃.

2.2. Structural characterization

Scanning electron microscope (SEM, JEOL, Model JSM-7600F) was used to observe the micromorphology of powder samples. The sample structure was performed by X-ray powder diffraction (XRD) on a Bruker AXS D8 Advance X-ray diffractometer using Cu Kα radiation (λ=0.15418 nm), scanning range of 10-80° and scanning rate of 10 ℃ min^{-1}.

2.3. Electrochemical measurements

In this study, an electrochemical workstation was used to evaluate the electrochemical performance of electrode materials. Firstly, FeS_2 powder sample (15 mg), conductive agent acetylene black (4.29 mg), and binder polyvinylidene fluoride (2.14 mg) were mixed at the ratio of 7:2:1. Then, add an appropriate amount of N-methylpyrrolidone solvent (100 mg), stir, and mix well. After weighing and recording the mass of blank graphite paper, the graphite paper with an area of 1 cm × 2 cm was coated with the mixed uniform sample, dried in a vacuum oven at 80 ℃ for 5 h, and then cooled to room temperature, then the working electrode was made and weighed. Three electrode system was used to test the electrochemical performance. The working electrode was the prepared electrode material, the reference electrode was Ag/AgCl electrode, and the counter electrode was a platinum electrode. The instrument is the ChI760E electrochemical workstation produced by Shanghai Chenhua Instrument Co., Ltd. to test the electrochemical performance of electrode materials at room temperature. The electrolyte is a newly prepared 1 mol/L sodium sulfate solution.

3. RESULTS AND DISCUSSION

The schematic diagram of hydrothermal synthesis of carbon-coated FeS_2 (C@ FeS_2) is illustrated in Fig. 1. Briefly, the hydrothermal method is used to synthesize FeS_2 with sodium thiosulfate, ferrous sulfate, and sublimed sulfur as raw materials. The effects of surfactants (PVP, CTAB, PEG) on the

morphology, structure, and electrochemical performance of FeS_2 synthesized by the hydrothermal method are discussed.

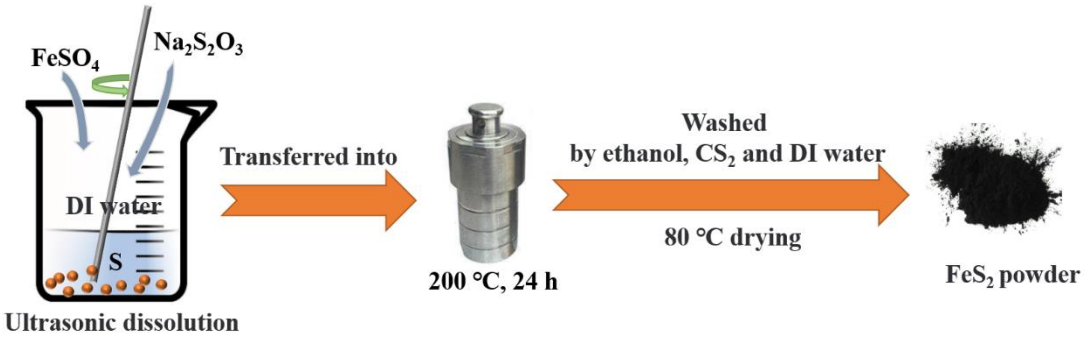

Figure 1. A simple schematic diagram of the synthesis of FeS_2.

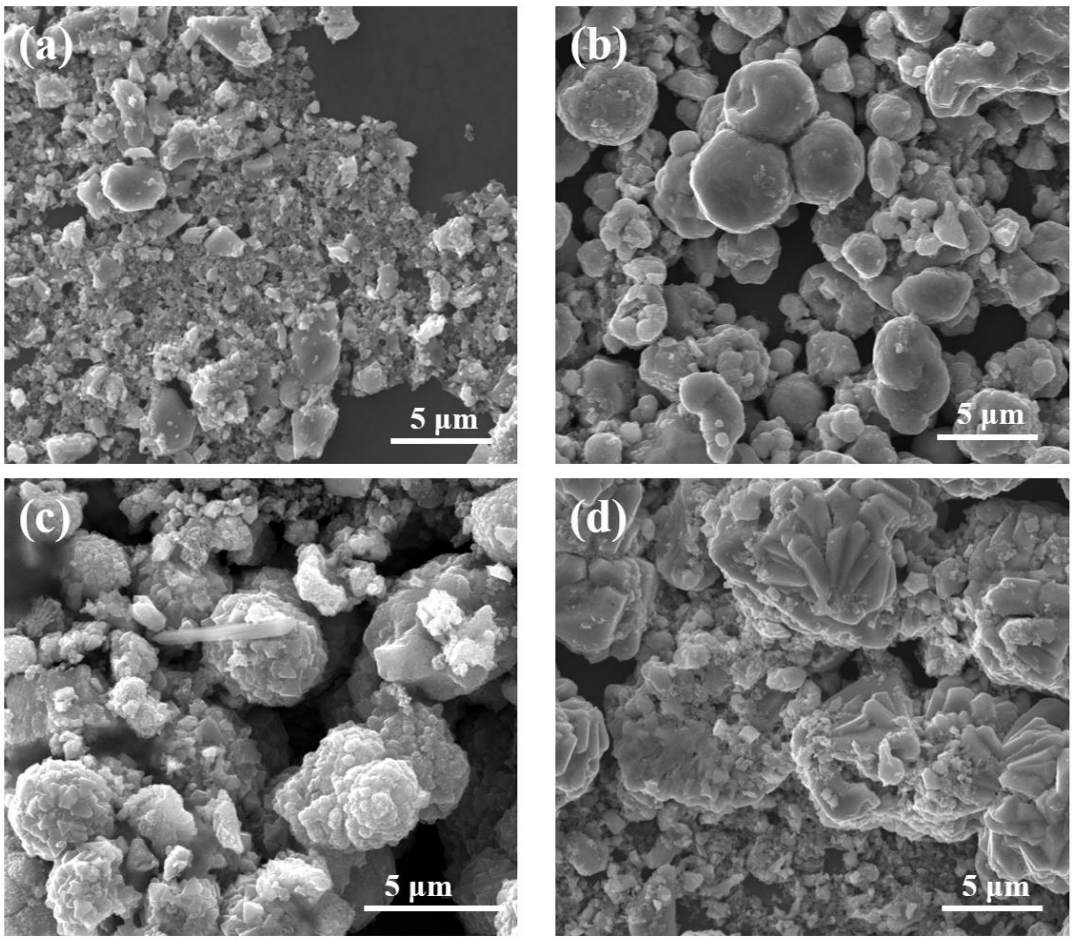

Figure 2. SEM images of FeS_2 powders prepared (a) without surfactant; (b) with PVP; (c) with CTAB and (d) with PEG.

Fig. 2(a) shows the field emission scanning electron microscope (SEM) image of FeS_2 powder prepared without surfactant. Obviously, the prepared sample particles have larger lumps and powders,

with a particle size of about 1-3 μm, at the micro-nano level. It is speculated that this may be related to the two structures. SEM of FeS_2 powder prepared by adding 40 mg PVP is depicted in Fig. 2(b). The cubic pyrite particles prepared by adding PVP are quasi-circular, with a particle size of 1-5 μm. Combining XRD analysis and comparison of SEM images without surfactants, it can be seen that it is precise because PVP promotes crystal growth in different directions to modify the surface shape of pyrite particles, which is crystal growth and morphology of pyrite are greatly affected by PVP. Fig. 2(c) gives SEM of FeS_2 powder prepared by adding 40 mg CTAB. The pyrite particles prepared by adding CTAB have a tooth-shaped spherical shape, with a particle diameter between 1-3 μm, and the size is relatively uniform, at the micro-nano level. Fig. 2(d) exhibits an SEM image of FeS_2 powder prepared by adding 40 mg PEG. The pyrite particles prepared by adding PEG are in the shape of flower buds, with a particle diameter of about 5 μm, relatively uniform in size, and the particles are of the micron level. From the comparison of SEM images, it is found that FeS_2 crystal growth and morphology are more significantly affected by PEG. And this method has not been found in other documents, and more detailed research will be done on its formation mechanism and electrochemical performance.

Fig. 3(a) exhibits the X-ray diffraction (XRD) pattern of FeS_2 powder prepared without surfactant. Some of the diffraction peaks correspond to the standard card (PDF#65-2567) with the space group Pnnm, and the FeS_2 of the orthorhombic system is marcasite; the other diffraction peaks correspond to the space group Pa-3. The standard card (PDF#65-3321) of the cubic crystal system of FeS_2 is pyrite; the main peak intensity of X-ray diffraction of FeS_2 samples prepared without surfactants corresponds to the crystal planes (110), (111), (200), (101), (210), (120), (211), (220), (211), (002), (311), (031), and there are no obvious spurious peaks.

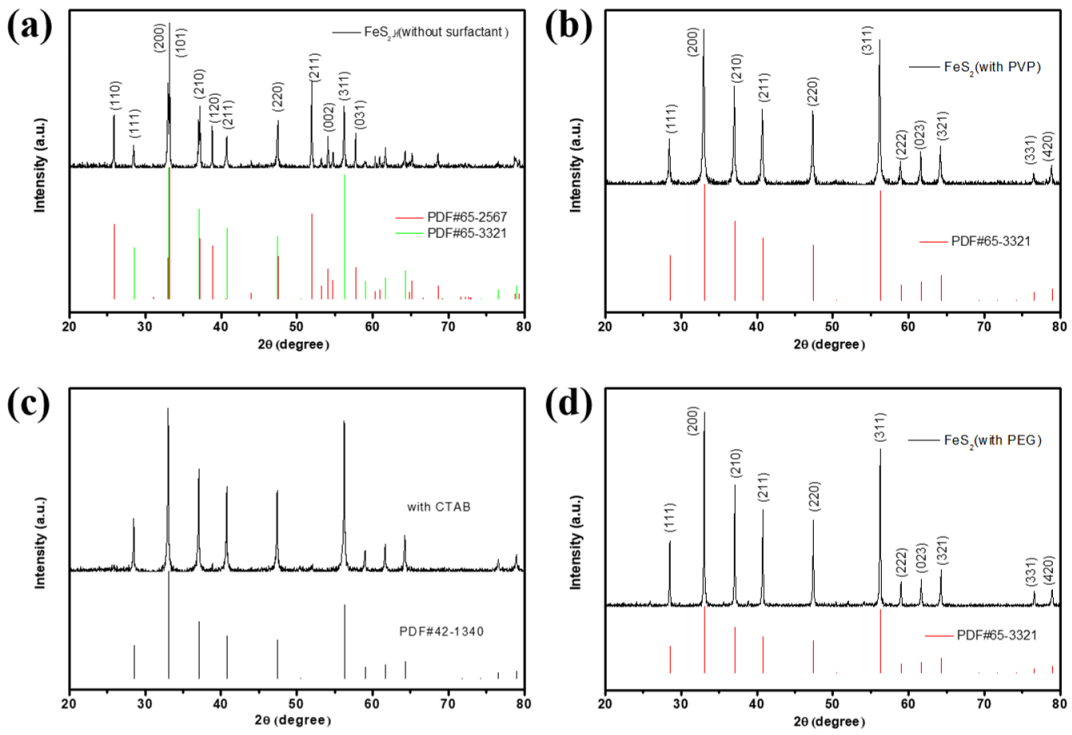

Figure 3. XRD patterns of FeS_2 powders prepared (a) without surfactant; (b) with PVP; (c) with CTAB and (d) with PEG.

From these peaks, it can be seen from the strength and half-height width that the FeS_2 samples we synthesized have good crystallinity. The results show that FeS_2 synthesized without surfactants has two space groups, Pa-3 and Pnnm, corresponding to two substances: cubic pyrite and orthorhombic marcasite, and in the experiment obviously found in the presence of white lumps. However, the crystal structure of FeS_2 synthesized by the solvent method is the only pyrite, reported by Venkateshalu et al. [10], which indicates that the synthesis method affects the structure of the final product. Fig. 3(b) provides XRD of FeS_2 powder prepared by adding 40 mg PVP. All the diffraction peaks correspond to the standard card (PDF#65-3321) with the space group Pa-3, corresponding to the lattice constant a=0.5419 nm, which indicates that the FeS_2 we prepared has a single cubic crystal. The structure is pyrite; the main peak intensity of FeS_2 sample prepared by adding PVP corresponds to crystal planes (111), (200), (210), (211), (220), (311), (222), (023), (321), (331), (420), and there are no obvious impurity peaks. From the intensity and half-height width of these peaks, it can be seen that the FeS_2 samples we synthesized have high crystallinity. Compared with the XRD comparison chart of the samples without surfactant and with FeS_2, it is found that the peak intensity of the two samples in the cubic crystal form of pyrite (200) is almost the same, while the sample prepared with PVP is in the cubic crystal form of pyrite (111), (210), (211), (220), (311) planes are stronger than FeS_2 samples prepared without surfactants, indicating that PVP promotes the growth of cubic pyrite crystals [9]. The results show that the introduction of PVP inhibits the formation of orthorhombic marcasite and promotes the growth of cubic pyrite crystals.

XRD of FeS_2 powder prepared by adding 40 mg CTAB is given in Fig. 3(c). All diffraction peaks correspond to the standard card (PDF#42-1340) with the space group Pa-3, corresponding to the lattice constant a=0.5418 nm. This indicates that the FeS_2 prepared by us has a single crystal structure and is cubic pyrite; the main peak intensity of the FeS_2 sample prepared by adding 40 mg CTAB corresponds to the crystal planes (111), (200), (210), (211), (220), (311), (222), (023), (321), (331), (420), and there are no obvious spurious peaks. From the intensity and half-height of these peaks, it can be seen that the FeS_2 sample we synthesized has high crystallinity. Compared with the XRD spectra of FeS_2 powder prepared without surfactants, it can be seen that the cubic pyrite prepared by adding CTAB peak intensities are significantly higher than that without surfactants, which shows that the introduction of CTAB not only inhibits the synthesis of orthorhombic marcasite but also promotes the growth of cubic pyrite crystals. Fig. 3(d) shows the XRD pattern of FeS_2 powder prepared by adding 40 mg PEG. All diffraction peaks correspond to the standard card with space group Pa-3 (PDF#65-3321), corresponding to the lattice constant a=0.5419 nm, which indicates that the FeS_2 we prepared has a single cubic crystal structure, is pyrite; the main peak intensity of X-ray diffraction of FeS_2 sample prepared by adding 40 mg PEG corresponds to crystal planes (111), (200), (210), (211), (220), (311), (222), (023), (321), (331), (420), and there are no obvious impurity peaks. From the intensity and half-height width of these peaks, we can see that the FeS_2 samples we synthesized have a very high crystallinity degree. Compared with the XRD comparison chart of FeS_2 samples prepared without surfactants and added PVP, it can be seen that the cubic pyrite prepared by adding PEG peak intensities are significantly higher than that of the other two materials, which shows that the introduction of PEG not only inhibits the synthesis of orthorhombic marcasite but also promotes the crystal orientation growth of cubic pyrite. In conclusion, the surfactant can change the crystal structure of FeS_2 [9].

To evaluate the electrochemistry properties, the cyclic voltammetry (CV) of FeS_2 electrode materials prepared with four different surfactants at different scan rates (5 mV/s, 10 mV/s, 50 mV/s, 80 mV/s, 100 mV/s) were provided in Fig. 4. In this experiment, CV was tested in a newly configured 1 mol/L sodium sulfate electrolyte solution, and the voltage window was -0.9~0 V. The masses of electrode active materials on FeS_2 electrode materials prepared by four different surfactants were 3.38 mg, 3.69 mg, 2.11 mg, and 3.58 mg, respectively. It can be seen from Fig. 4 that CV curves at all scan rates have no obvious redox peaks, indicating Faraday pseudo-capacitance [22]. The symmetry of the CV curve is good, indicating that the reaction process of the electrode active material on the electrode surface is reversible [23].

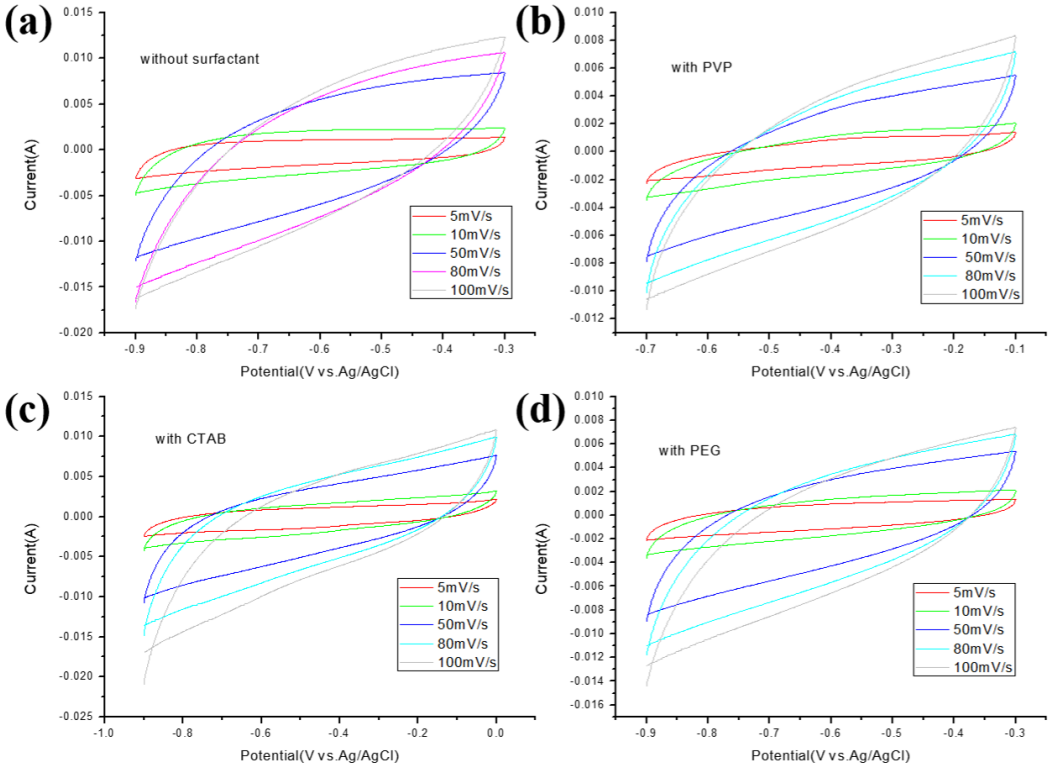

Figure 4. CV curves of FeS_2 electrode material prepared by (a) without surfactant; (b) with PVP; (c) with CTAB and (d) with PEG in the voltage range of -0.9-0 V at scan rates of 5, 10, 50, 80 and 100 mV/s, respectively.

Fig. 4(a) implies that the integrated area of the CV curve of the same electrode material increases with the increase of the scan rate, and the larger the integrated area, the smaller the integrated value. According to the specific capacitance calculation formula (1) in the CV curve, it can be estimated that with the increase of the scan rate, the specific capacitance of the electrode decreases with the same electrode material. The reason is that when the scan rate increases, it will prevent ions from approaching on the electrode. And transfer, the ion concentration at the interface between the electrode and the electrolyte solution increases rapidly, and the diffusion speed of the electrolyte from the solid/liquid interface to the inside of the electrode material is insufficient to meet the electrochemical reaction of the electrode material, so that when the current increases, the utilization rate of the active material decreases,

leading to a decrease in specific capacitance [24]. The calculation formula of specific capacitance in the CV curve is as follows [11, 25]:

$$Cs=\int I(V)dV / v(V\,\max - V\,\min)m \quad (1)$$

Where, $\int I(V)dV$ is the enclosed area of CV, (V max-V min) is the voltage window (V), m is the mass of the electrode active material (mg), and v is the scan rate (V/s).

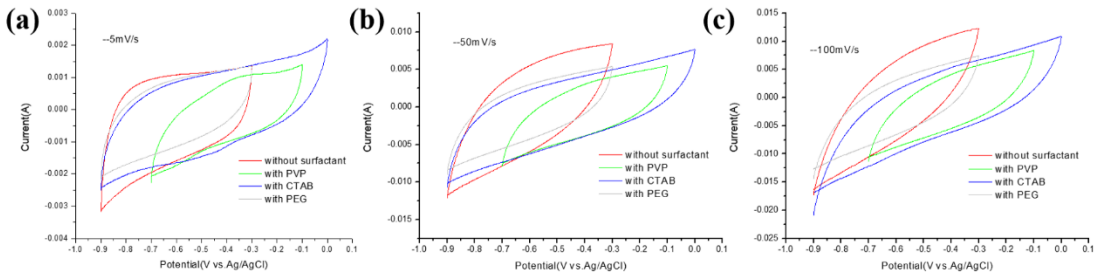

Figure 5. CV comparison of FeS_2 electrode materials prepared by different surfactants (surfactant free, PVP, CTAB and PEG) in the voltage range of -0.9-0 Vat (a) 5 mV/s; (b) 50 mV/s and (c) 100 mV/s.

Fig. 5(a) displays the comparison of the CV of electrode materials prepared with four different surfactants at 5 mV/s. The integrated area of the volt-ampere curve can be calculated by Origin. For FeS_2 electrode material without surfactant, the integrated area at a scan rate of 5 mV/s is 0.00526 and the specific capacitance is 141.03 F/g; the integrated area of the FeS_2 electrode material prepared by adding PVP at a scan rate of 5 mV/s is 0.00323 and the specific capacitance is 82.20 F/g; the integrated area of the FeS_2 electrode material prepared by adding CTAB at a scan rate of 5 mV/s is 0.00623, and the specific capacitance is 191.68 F/g, and the integrated area of the FeS_2 electrode material prepared by adding PEG at a scan rate of 5 mV/s is 0.00349, the specific capacitance is 134.37 F/g. Fig. 5(b) shows the CV comparison diagram of four kinds of electrode materials prepared by different surfactants at 50 mV/s. The integral area with PEG is larger than that without surfactant. According to the specific capacitance calculation formula (1), it can be estimated that the specific capacity without surfactant is greater than that with PEG. According to the integral area of CV curve, the specific capacitance of FeS_2 electrode material at 50 mV/s scanning rate can be calculated as 51.87 F/g, 29.18 F/g, 65.61 F/g, and 45.09 F/g, respectively, which is consistent with the estimated values. In terms of specific capacitance, the electrochemical performance of FeS_2 electrode material prepared by adding CTAB is excellent. Fig. 5(c) provides the CV comparison diagram of electrode materials prepared by four different surfactants at 100 mV/s. According to formula (1) and origin integral, the specific capacitances of electrode materials prepared by four different surfactants at 100 mV/s are 31.07 F/g, 19.87 F/g, 42.65 F/g, and 28.42 F/g, respectively. By a comparison, a higher decreasing capacitance rate was observed with increasing scan rates from 5 to 100 mV s^{-1} due to the existence of the complete diffusion of electrolyte ions at a lower scan rate resulting in higher charge storage [9, 10, 17].

The frequency range of the electrochemical impedance (EIS) test is 0.1 Hz to 100000 Hz, and the open-circuit voltage is 5 mV. EIS is a Nyquist curve, which consists of two parts: a semicircle in the high-frequency region and a straight line in the low-frequency region [26]. The semicircle in the high-frequency region represents the internal charge transfer resistance (*Rs*). The larger the diameter of the semicircle, the greater the charge transfer resistance; the Warburg impedance of the linear electrode material in the low-frequency region represents the diffusion speed of the electrolyte in the electrode (*W1*). Fig. 6 is an EIS comparison diagram of FeS_2 electrode materials prepared by four different surfactants. In the high-frequency region, it can be seen that the four different surfactants prepared FeS_2 electrode materials are all the appearance of a semi-circular arc indicates that there is a certain charge transfer resistance in the electrolyte.

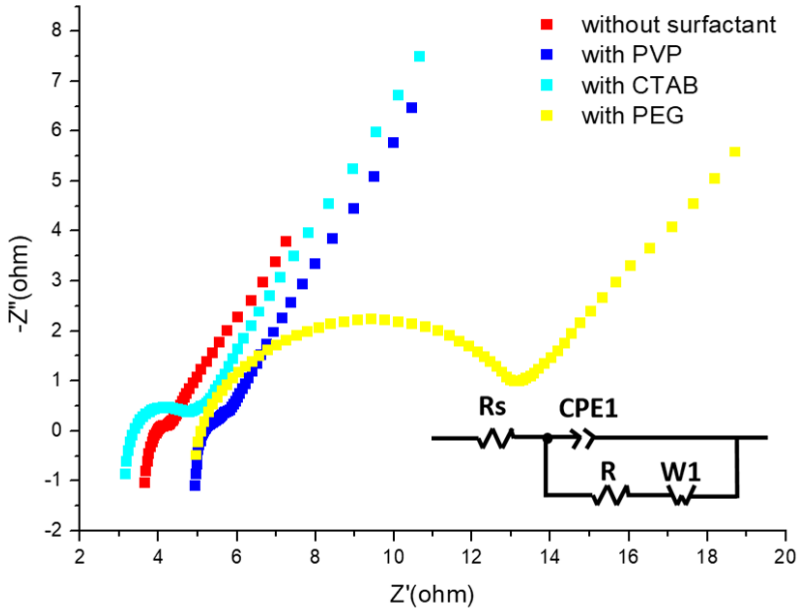

Figure 6. Electrochemical impedance comparison and corresponding fitted equivalent circuit model (inset) of FeS_2 electrode materials prepared by four different surfactants (surfactant-free, PVP, CTAB, and PEG) over the frequency range of 100 kHz to 0.1 Hz in a 1 M Na_2SO_4 solution.

Table 1. The calculated internal charge transfer resistance (*Rs*).

	Without surfactant	PVP	CTAB	PEG
Rs/Ω	3.95	3.97	3.71	7.12

Table 1 gives the calculated internal charge transfer resistance (*Rs*). The resistances of four surfactants (surfactant-free, PVP, CTAB, and PEG) are 3.95, 3.97, 3.71, and 7.12 Ω, respectively. It is obvious that the diameter of the semicircular arc of the FeS_2 electrode material prepared by adding PEG is the largest, indicating that the FeS_2 electrode material has the highest charge transfer resistance (*Rs*=7.12 Ω) and the lowest electron migration rate. In addition, SEM proves that particles of FeS_2 with

PEG are largest than the other three surfactants, which explain well FeS_2 with PEG has poor electrochemistry properties. In short, the introduction of PEG promotes the overgrowth of cubic pyrite and forms a micron level, bud-shaped spherical particles. Therefore, to obtain better performance, two strategies can be adopted [27, 28]. One is nanoization, which improves the experimental synthesis conditions to synthesize nanoscale particles, which is more conducive to ion diffusion. On the other hand, carbon coating improves electronic conductivity. For example, Golsheikh et al. [29] constructed FeS_2 (pyrite)/graphene nanocomposite, and Lu et al. [30] synthesized metal-organic framework-derived sea-cucumber-like FeS_2@C nanorods.

4. CONCLUSIONS

In this study, high purity FeS_2 was synthesized by the hydrothermal method using sodium thiosulfate, ferrous sulfate, and sublimated sulfur as raw materials. The effects of different surfactants on the morphology and electrochemical properties of FeS_2 synthesized by the hydrothermal method were discussed. The morphology and structure were analyzed by XRD and SEM, and the electrochemical performance was carried out by electrochemical workstation performance test. According to the analysis of the CV curve, the electrochemical reactions of FeS_2 prepared by four different surfactants (without surfactant, PVP, CTAB, and PEG) were reversible. The specific capacitance is 141.03 F/g, 82.20 F/g, 191.68 F/g, 134.37 F/g at 5 mV/s scanning rate, and 51.87 F/g, 29.18 F/g, 65.61 F/g and 45.09 F/g at 50 mV/s scanning rate, respectively The results of electrochemical impedance test show that FeS_2 prepared without surfactant, PVP and CTAB have lower charge transfer impedance and higher ion diffusion, which is attributed to the nanoscale FeS_2 prepared, which shortens the ion diffusion path and promotes the electrode reaction kinetics. However, PEG promoted FeS_2 crystal overgrowth to form micron-sized particles, so it has a poor electrochemical performance.

ACKNOWLEDGMENTS
This research was funded by Natural Science Foundation of Guangdong Province (Grant No. 2017A03031057), University Natural Science Research Project of Anhui Province (Grant No. KJ2019A1278) and Anhui Provincial Quality Project (Grant No.2018ylzy159).

References

1. M.Z. Jacobson, M.A. Delucchi, Z.A. Bauer, S.C. Goodman, W.E. Chapman, M.A. Cameron, C. Bozonnat, L. Chobadi, H.A. Clonts, P. Enevoldsen, *Joule*, 1 (2017) 108.
2. J. Zhao, G. Zhou, K. Yan, J. Xie, Y. Li, L. Liao, Y. Jin, K. Liu, P.C. Hsu, J. Wang, H.M. Cheng, Y. Cui, *Nat. Nanotechnol.*, 12 (2017) 993.
3. J.B. Goodenough, Y. Kim, *Chem. Mater.*, 22 (2010) 587.
4. C. Yang, J. Chen, X. Ji, T.P. Pollard, X. Lu, C.J. Sun, S. Hou, Q. Liu, C. Liu, T. Qing, Y. Wang, O. Borodin, Y. Ren, K. Xu, C. Wang, *Nature*, 569 (2019) 245.
5. J.-N. Zhang, Q. Li, C. Ouyang, X. Yu, M. Ge, X. Huang, E. Hu, C. Ma, S. Li, R. Xiao, W. Yang, Y. Chu, Y. Liu, H. Yu, X.-Q. Yang, X. Huang, L. Chen, H. Li, *Nature Energy*, 4 (2019) 594.

6. J. Liu, Y. Lu, Z. Xu, R. Wang, X. Li, *Int. J. Electrochem. Sci.*, 15 (2020) 1509.
7. X. Zhang, K. Ding, X. Gao, X. Shi, J. Han, J. Pan, *Int. J. Electrochem. Sci*, 15 (2020) 1498.
8. X. Shen, Y. Li, T. Qian, J. Liu, J. Zhou, C. Yan, J.B. Goodenough, *Nat. Commun.*, 10 (2019) 900.
9. I.K. Durga, S.S. Rao, R.M.N. Kalla, J.-W. Ahn, H.-J. Kim, *J. Energy Storage*, 28 (2020) 101216.
10. S. Venkateshalu, P.G. Kumar, P. Kollu, S.K. Jeong, A.N. Grace, *Electrochim. Acta*, 290 (2018) 378.
11. L.L. Zhang, X. Zhao, *Chem. Soc. Rev.*, 38 (2009) 2520.
12. J. Yan, Y.-Y. Fang, S.-W. Wang, S.-D. Wu, L.-X. Wang, Y. Zhang, H.-W. Luo, Y. Cao, H.-L. Gao, L.-Z. Wang, *Int. J. Electrochem. Sci*, 15 (2020) 1982.
13. W.-D. Yang, Y.-J. Lin, *Int. J. Electrochem. Sci*, 15 (2020) 1915.
14. T. Zhao, S. Guo, X. Ji, Y. Zhao, X. Wang, Y. Cheng, J. Meng, *Fuller. Nanotub. Car. N.*, 25 (2017) 391.
15. H. Liu, Z. Lu, J. Qin, K. Wang, F. Feng, Y. Guo, *Fuller. Nanotub. Car. N.*, 27 (2019) 947.
16. H. Liu, Q. Zhao, K. Wang, Z. Lu, F. Feng, Y. Guo, *Fuller. Nanotub. Car. N.*, 27 (2019) 661.
17. L. Pei, Y. Yang, H. Chu, J. Shen, M. Ye, *Ceram. Int.*, 42 (2016) 5053.
18. M.S. Javed, Z. Jiang, C. Zhang, L. Chen, C. Hu, X. Gu, *Electrochim. Acta*, 219 (2016) 742.
19. L. Li, M. Cabán-Acevedo, S.N. Girard, S. Jin, *Nanoscale*, 6 (2014) 2112.
20. X. Feng, X. He, W. Pu, C. Jiang, C. Wan, *Ionics*, 13 (2007) 375.
21. B. Balakrishnan, S.K. Balasingam, K.S. Nallathambi, A. Ramadoss, M. Kundu, J.S. Bak, I.H. Cho, P. Kandasamy, Y. Jun, H.-J. Kim, *J. Ind. Eng. Chem.*, 71 (2019) 191.
22. W. Luo, H. Xue, *Fuller. Nanotub. Car. N.*, 27 (2019) 189.
23. V. Sridhar, H. Park, *J. Alloys Compd.*, 732 (2018) 799.
24. Y. Zhong, J. Liu, Z. Lu, H. Xia, *Mater. Lett.*, 166 (2016) 223.
25. W. Raza, F. Ali, N. Raza, Y. Luo, K.-H. Kim, J. Yang, S. Kumar, A. Mehmood, E.E. Kwon, *Nano Energy*, 52 (2018) 441.
26. Z. Sun, H. Lin, F. Zhang, X. Yang, H. Jiang, Q. Wang, F. Qu, *J. Mater. Chem. A*, 6 (2018) 14956.
27. H. Li, P. Wu, Y. Xiao, M. Shao, Y. Shen, Y. Fan, H. Chen, R. Xie, W. Zhang, S. Li, J. Wu, Y. Fu, B. Zheng, W. Zhang, F. Huo, *Angew. Chem. Int. Ed.*, 59 (2020) 4763.
28. J. Leng, Z. Wang, J. Wang, H.H. Wu, G. Yan, X. Li, H. Guo, Y. Liu, Q. Zhang, Z. Guo, Chem. *Soc. Rev.*, 48 (2019) 3015.
29. A. Moradi Golsheikh, N.M. Huang, H.N. Lim, C.H. Chia, I. Harrison, M.R. Muhamad, *Chem. Eng. J.*, 218 (2013) 276.
30. Z. Lu, N. Wang, Y. Zhang, P. Xue, M. Guo, B. Tang, X. Xu, W. Wang, Z. Bai, S. Dou, *ACS Appl. Energy Mater.*, 1 (2018) 6234.